Noncovalent Interactions between Unsolvated Peptides†

David T. Kaleta and Martin F. Jarrold*

Department of Chemistry, Northwestern University, 2145 Sheridan Road, Evanston, Illinois 60208

Received: January 23, 2002; In Final Form: April 23, 2002

The conformations of the unsolvated dimers and trimers produced by electrospraying mixtures of polyalanine-based peptides have been examined using ion mobility measurements in conjunction with molecular dynamics simulations. These multimers can provide models for how the secondary structure associates into the motifs that makeup the tertiary structure domains of proteins. Mixtures of helix-forming monomers ($Ac-A_{14}K$ and $Ac-A_{15}K$ and $Ac-(GA)_7K$ and $Ac-A(GA)_7K$; Ac = acetyl, G = glycine, A = alanine, and K = lysine) yield V-shaped helical dimers where the C termini are tethered together by the protonated lysine side chain from one peptide interacting with the C terminus of the other (exchanged lysines). Trimers from the $Ac-(GA)_7K$ and $Ac-A(GA)_7K$ mixture adopt a pinwheel arrangement of helices with all three C termini tethered together by exchanged lysines. Trimers are much less abundant for the $Ac-A_{14}K$ and $Ac-A_{15}K$ mixture. The V-shaped dimer and pinwheel trimer arrangement leads to a cooperative electrostatic stabilization of the helices through the interaction of the combined charge with the helix dipoles. Mixtures of globule-forming monomers ($Ac-K(GA)_7$ and $Ac-KA(GA)_7$) form predominantly globular multimers. In some conformations, however, the helical state is stabilized by interactions with the local environment. Examples include the antiparallel arrangement of helices that is present as a minor component for the $Ac-K(GA)_7 \cdot Ac-KA(GA)_7+2H^+$ dimer and dominant for the $Ac-KA_{14} \cdot Ac-KA_{15}+2H^+$ dimer, as well as conformations with one or more helices which occur for the trimers from the $Ac-K(GA)_7$ and $Ac-KA(GA)_7$ mixture.

Introduction

Many amino acids display a propensity to adopt particular conformations. For example, alanine is a helix former and valine has a high propensity to make β sheets. The resulting secondary structure elements assemble through noncovalent interactions to ultimately give the three-dimensional structure of a protein. A small palette of naturally occurring amino acids are enough to form the myriad of functional entities that drive life itself, but the connection between the sequence and structure is poorly understood. A wealth of information has been obtained from studies of proteins and peptides in solution. However, the solution phase conformations are influenced by the solvent, and it is often difficult to unravel the complex interplay between intramolecular and solution interactions.[1] Furthermore, the aqueous solution is not the only biologically important environment; membrane proteins comprise up to 30% of all proteins encoded by genomes,[2] and the hydrophobic interior of a lipid bilayer is strikingly different from the environment inside and outside of the cell membrane. A new approach to understanding protein structure has recently emerged which is based on determining the intrinsic properties without the influence of external environmental interactions. This then provides a foundation for understanding protein and peptide action throughout the biological milieu. As part of this effort, there have been a number of studies of the conformations of unsolvated peptides and proteins.[3] Our recent efforts have focused on examining helix formation in unsolvated peptides and, in particular, determining intrinsic helix propensities.[4,5]

In the work described here, we take the next logical step and begin to investigate the aggregation of monomeric peptides into multimers. These multimers can provide models for how secondary structure associates into motifs, which then go on to assemble into the tertiary structure domains of proteins.[6] In addition, the interactions between monomeric peptides have been investigated as a model for understanding the formation of ion channels,[7−9] which are an important structure in biological cell membranes and in the action of antipathogenic drugs. Peptaibols,[10] for example, are antibiotic peptides of fungal origin that make pores in cell membranes by associating to form an aggregate of transmembrane helices.

In the work described here, we have examined the conformations of a variety of unsolvated peptide dimers and trimers produced by electrospray. Electrospray[11] is a sufficiently gentle ionization technique that weakly bound noncovalent complexes can be transferred into the gas phase,[12−14] and the observation of peptide aggregates is fairly common.[15−17] The conformations of the noncovalent complexes were probed using ion mobility measurements. The mobility of a gas phase ion depends on its average collision cross section which in turn depends on its structure. Ions with compact folded structures travel more rapidly than ions with more open conformations. For example, this approach can distinguish between helices and globules for unsolvated monomeric peptides.[18]

The specific peptides studied here are as follows: $Ac-(GA)_7K$ and $Ac-A(GA)_7K$, $Ac-K(GA)_7$ and $Ac-KA(GA)_7$, $Ac-KA_{14}$ and $Ac-KA_{15}$, $Ac-A_{14}K$ and $Ac-A_{15}K$ (Ac = acetyl, G = glycine, A = alanine, and K = lysine). Mixtures of peptides that differ by one residue are studied so that the mixed dimers and trimers (which are multiply charged) have a unique mass-to-charge ratio. Previous work has shown that the monomeric peptides with a C-terminus lysine are predominantly helical, whereas those with an N-terminus lysine are predominantly globular (a random-looking three-dimensional struc-

† Part of the special issue "Jack Beauchamp Festschrift".

* To whom correspondence should be addressed.

10.1021/jp020227b CCC: $22.00
Published on Web 07/10/2002

ture).[18,19] This difference is attributed to the location of the protonated lysine. With a C-terminus lysine, the helical state is stabilized by favorable interactions between the protonated lysine side chain and the helix dipole, whereas with the N-terminus lysine, this interaction destabilizes the helical state. The glycine residues are expected to destabilize the helical state in the Ac−$(GA)_7$K and Ac−A$(GA)_7$K peptides relative to that in the all-alanine analogues. To complement the experimental studies, a series of molecular dynamics (MD) simulations were performed. The simulations provide cross sections for comparison to those derived from the ion mobility measurements. A preliminary account of some aspects of this work has been given.[20]

Materials and Methods

Peptide Synthesis. The peptides were synthesized using *FastMoc* (a variant of Fmoc) chemistry with an Applied Biosystems model 433A peptide synthesizer. After synthesis, the peptides were cleaved from the solid substrate with a 95% trifluoroacetic acid (TFA)/5% water solution, precipitated from solution with cold ethyl ether, washed, and lyophilized. Solutions of 1−2 mg of each peptide in 1 mL of 90% TFA/10% water were electrosprayed.

Ion Mobility Measurements. The ion mobility apparatus has been described previously.[21] It consists of an electrospray source, a 30.5 cm long drift tube, quadrupole mass spectrometer, and detector. Ions are electrosprayed in air and enter the apparatus through a stainless steel capillary set into a heated copper−beryllium block. The capillary ends in a differentially pumped region which is maintained at around 0.2 Torr, and some of the ions pass through this region and into the main chamber where they are focused into the drift tube. The drift tube is operated with a helium buffer gas pressure of approximately 4 Torr and a drift voltage of 380 V. At the end of the drift tube, some of the ions exit through a small aperture and are then focused into a quadrupole mass spectrometer where they are mass analyzed. The transmitted ions are then detected by an off-axis collision dynode and dual microchannel plates.

Drift time distributions are obtained using an electrostatic shutter to admit short (50 or 100 μs) packets of ions into the drift tube. A multichannel scaler, synchronized with the electrostatic shutter, is used to record the arrival time distribution for mass selected ions at the detector. The drift time distribution is then obtained by correcting the arrival time distribution for the time the ions spent traveling outside of the drift tube. The measured drift times are converted into collision cross sections using[22]

$$\Omega_{avg}^{(1,1)} = \frac{(18\pi)^{1/2}}{16}\left[\frac{1}{m}+\frac{1}{m_b}\right]^{1/2}\frac{ze}{(k_B T)^{1/2}}\frac{t_D E}{L}\frac{1}{\rho} \qquad (1)$$

where m and m_b are the masses of the ion and buffer gas atom respectively, ze is the ion's charge, ρ is the buffer gas number density, L is the length of the drift tube, and E is the drift field.

Molecular Dynamics Simulations. Information about the nature of the conformations present in the drift time distributions is obtained by comparing the measured values to orientationally averaged cross sections calculated for geometries obtained from molecular dynamics (MD) simulations. The MD simulations were performed with the MACSIMUS suite of programs[23] using CHARMM potentials (21.3 parameter set)[24] with a dielectric constant of 1.0 and time step of 1 fs. A friction thermostat was employed, and the kinetic energies were rescaled every 0.1 ps to maintain the temperature. Bond lengths were constrained by SHAKE,[25] and CH, CH_2, and CH_3 groups were treated as united atoms.[26]

A series of simulations were performed for the monomeric peptides to confirm their conformations, obtain energies for the different conformations, and provide low energy geometries to construct some initial conformations for the dimers and trimers. Five 300 K 960 ps MD simulations were performed for each monomeric peptide starting from an α helix ($\phi = -57°$ and $\psi = -47°$). In addition, a series of simulated annealing[27] runs were performed for each monomer starting from both an α helix and a fully extended, all-trans conformation. The annealing schedule consisted of 100 or 240 ps at 600 K, followed by 240 ps at 500 K, 240 ps at 400 K, and 480 ps at 300 K. In previous work, these relatively gentle annealing schedules seemed to do best at the difficult task of locating compact low-energy globule conformations.[28] At least 30 simulated annealing runs were performed for each monomer starting from an extended all-trans geometry, and at least 10 simulated annealing runs were performed starting from an α helix. Only two types of conformation were found: an extended helix and a globule (a random-looking three-dimensional structure which in some cases may incorporate a short helical section). For peptides with a lysine at the N terminus, the helix does not survive the simulations, but it collapses into a globule. For peptides with a lysine at the C terminus, the helix is stable, and the protonated lysine side chain loops around and hydrogen bonds to the dangling carbonyl groups at the C terminus. An analogous helix capping effect often occurs in proteins.[29,30] The helices are predominantly α helices with a tendency toward a partial π helix at the C terminus.

Starting conformations for MD simulations of the dimers and trimers were obtained by taking the monomer conformations and manipulating them by hand within a graphical environment. The monomer conformations employed were either ideal α helices or low energy globules from the monomer simulations. The starting conformations used for the dimers include coaxial helices (with the helix dipoles pointing in the same direction and in opposite directions), side-by-side helices (in both antiparallel and parallel orientations), and aggregates of two low energy globules. In addition, parallel, antiparallel, and collinear arrangements of linear, all-trans monomers were also used as starting points for MD simulations. A series of 10 300 K 960 ps simulations were performed for each initial configuration, and simulated annealing runs, using the schedule described above, were done for some of the initial configurations. The final conformations from these simulations were used as starting points for further 300 K 960 ps simulations or further simulated annealing runs. In addition, some 960 ps simulations were performed at elevated temperatures to test the stability of some of the resulting conformations.

For the helical peptides, there are two distinct arrangements for the lysine side chains. For isolated peptides with a C-terminus lysine, the protonated lysine side chain loops around and hydrogen bonds to the dangling carbonyl groups at the C terminus of the helix. We refer to this as self-solvated. Peptides with an N-terminus lysine cannot self-solvate in this way. The other distinct arrangement is where a protonated lysine from one peptide interacts with the C terminus of another helical peptide. We refer to this arrangement as exchanged, and it is possible for peptides with lysine at the N and C termini. When possible, simulations were done for both the self-solvated and exchanged arrangements. In general, the exchanged arrangement appeared to be slightly more stable. In some cases, simulations

that started as self-solvated switched to exchanged, but we never observed the exchanged arrangement to switch to self-solvated.

There are many more conformations for trimers than there are for dimers. Our starting conformations for the trimers include two different types of helical aggregates: planar, where all three helices are aligned side-by-side with each other in a plane, and nonplanar, where the helices are aligned side-by-side and closely packed. Both these groups have a variety of parallel and antiparallel arrangements of the helices, and these were all considered. Furthermore, there are various permutations associated with the placement of the 15- and 16-residue peptides. For example, 15−15−16, 15−16−15, 15−16−16, and 16−15−16 are all possible for the parallel planar arrangement. Most of these permutations were also considered. Other trimer starting conformations we examined include three α helices lying head-to-toe at the edges of a triangle and an extended coaxial arrangements of helices. All possible combinations in the orientation of the helix dipoles were considered. We also considered groupings of low energy globules. Finally, we examined side-by-side and coaxial arrangements of linear, all-trans monomers, and side-by-side β-sheet arrangement. These tended to make braid-like structures which were quite high energy. When appropriate, we examined both self-solvated and exchanged arrangements of the lysine side chains. A series of 10 300 K 960 ps simulations were performed for all of the initial conformations. Arrangements that produced particularly low energies were subjected to simulated annealing using the schedule described above. In a few cases, further 300 K 960 ps MD simulations were performed using the final conformation from the simulated annealing runs as the starting point. In addition, some 960 ps simulations were performed for a series of elevated temperatures to test the relative stability of selected trimer conformations with respect to dissociation.

Average energies and average collision cross sections were obtained from the final 35 ps of each simulation. Cross section were calculated using an empirical correction to the exact hard spheres scattering model,[28] averaging over 50 snapshots taken from the final 35 ps of each simulation. If the conformation is correct in the simulation, the calculated cross sections are expected to be within 2% of the measured values.

Results

The Monomers. For peptides with a C-terminus lysine, Ac−A_{14}K+H^+, Ac−A_{15}K+H^+, Ac−$(GA)_7$K+H^+, and Ac−$A(GA)_7$K+H^+, the dominant features present in the drift time distributions of the monomers are helical. The measured cross sections are within 2% of the cross sections calculated for helices from the MD simulations. Glycine is expected to destabilize the helical state and for both the Ac−$(GA)_7$K+H^+ and Ac−$A(GA)_7$K+H^+ monomers there were small features in the drift time distributions (∼15% of the helix intensity) with cross sections close to those expected for globules. Analogous features were not observed in the drift time distributions for Ac−A_{14}K+H^+ and Ac−A_{15}K+H^+. In the MD simulations, the helix was around 100 kJ mol^{-1} more stable than the globule for Ac−A_{14}K+H^+ and Ac−A_{15}K+H^+. This difference dropped to around 40 kJ mol^{-1} for Ac−$(GA)_7$K+H^+ and Ac−$A(GA)_7$K+H^+.

For peptides with an N-terminus lysine, Ac−KA_{14}+H^+, Ac−KA_{15}+H^+, Ac−K$(GA)_7$+H^+, and Ac−K$A(GA)_7$+H^+, the dominant features present in the drift time distributions of the monomers are globules. They have cross sections which are within 2% of the lowest energy globules found in the MD simulations. No evidence for a small component of an α-helical conformation was found for any of the peptides with an N-terminus lysine.

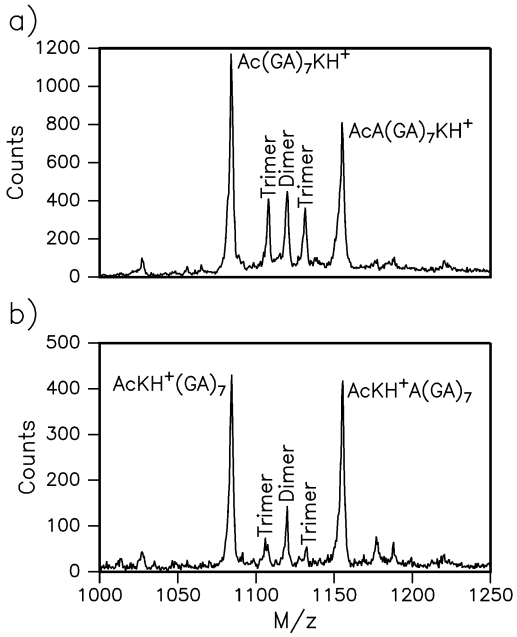

Figure 1. Electrospray mass spectra recorded for mixtures of (a) Ac−$(GA)_7$K and Ac−$A(GA)_7$K and (b) Ac−K$(GA)_7$ and Ac−K$A(GA)_7$ in 90%TFA/10% water. The peak for the low mass trimer in b (2Ac−K$(GA)_7$·Ac−K$A(GA)_7$+$3H^+$) overlaps with the peak due to Ac−K$(GA)_7$+Na^+.

Ac−$(GA)_7$K and Ac−$A(GA)_7$K Mixture. Figure 1a shows a typical mass spectrum obtained from electrospraying a 1:1 mixture of Ac−$(GA)_7$K and Ac−$A(GA)_7$K peptides with a capillary temperature of 60 °C. Abundant peaks due to the mixed dimer (Ac−$(GA)_7$K·Ac−$A(GA)_7$K+$2H^+$) and mixed trimers (2Ac−$(GA)_7$K·Ac−$A(GA)_7$K+$3H^+$ and Ac−$(GA)_7$K·2Ac−$A(GA)_7$K+$3H^+$) are evident between the Ac−$(GA)_7$K+H^+ and Ac−$A(GA)_7$K+H^+ peaks. Note that the Ac−$(GA)_7$K+H^+ and Ac−$A(GA)_7$K+H^+ peaks consist of monomers and homomultimers (dimers and trimers with the same mass-to-charge ratios as the monomers). Gentle electrospray conditions are required to observe the weakly bound dimers and trimers.[12,31] Higher capillary temperatures produced progressively lower multimer abundances until, at around 130 °C, only monomers were observed. Similar behavior was observed for all of the other peptides studied here.

Figure 2 shows the drift time distributions for the dimer and trimers evident in Figure 1a. The peaks in the drift time distributions are labeled (i) to (ix) for reference. The drift time distribution for the dimer shows three peaks: a narrow peak at long drift times which corresponds to a cross section of 485 $Å^2$, and two broader peaks at shorter drift times corresponding to cross sections around 379 $Å^2$ and 433 $Å^2$. The drift time distributions for the two trimers are quite similar, each showing three peaks: an intense peak at long drift times and two smaller peaks at shorter drift times. The cross sections for the light trimer (2Ac−$(GA)_7$K·Ac−$A(GA)_7$K+$3H^+$) are slightly smaller than the corresponding cross sections for the heavy trimer (Ac−$(GA)_7$K·2Ac−$A(GA)_7$K+$3H^+$).

Ac−K$(GA)_7$ and Ac−K$A(GA)_7$ Mixture. Figure 1b shows a typical mass spectrum for a 1:1 mixture of Ac−K$(GA)_7$ and Ac−K$A(GA)_7$ obtained using similar conditions to those used to record Figure 1a. The mass spectra for peptides with the N-terminus lysine exhibit a significantly reduced multimer

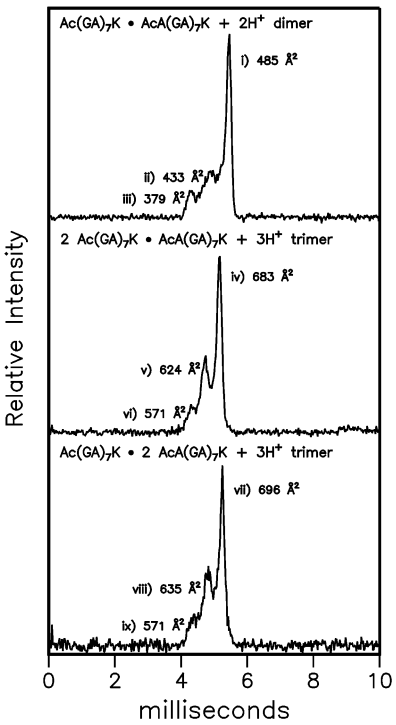

Figure 2. Drift time distributions recorded for the dimer and trimer ions obtained from the Ac−$(GA)_7$K and Ac−$A(GA)_7$K mixture. The main features in the drift time distributions are labeled i−ix for reference and assigned cross sections.

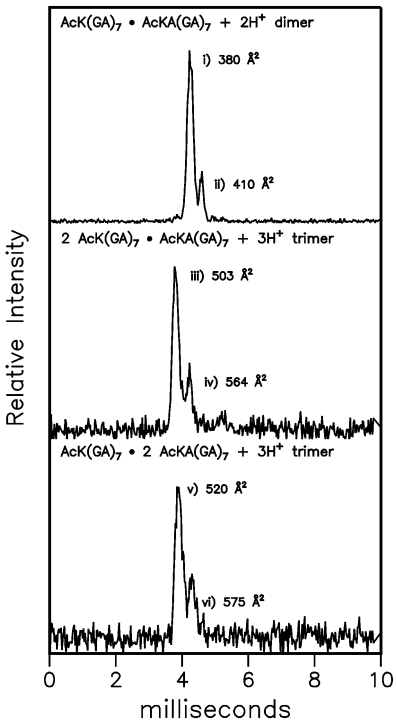

Figure 3. Drift time distributions recorded for the dimer and trimer ions obtained from the Ac−$K(GA)_7$ and Ac−$KA(GA)_7$ mixture. The main features in the drift time distributions are labeled i−vi for reference and assigned cross sections.

abundance compared with peptides with the C-terminus lysine. In particular, the abundance of the trimers is substantially reduced. Figure 3 shows drift time distributions recorded for the dimer and trimers. For both the dimer and trimers, two main features are resolved in the drift time distributions, and the dominant feature has the shorter drift time. The peaks are labeled (i) to (vi) for reference.

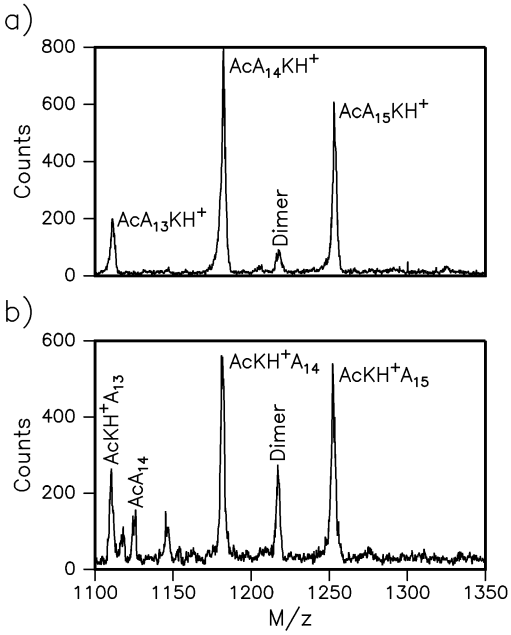

Figure 4. Electrospray mass spectra recorded for mixtures of (a) Ac−A_{14}K and Ac−A_{15}K and (b) Ac−KA_{14} and Ac−KA_{15} in 90%TFA/10% water.

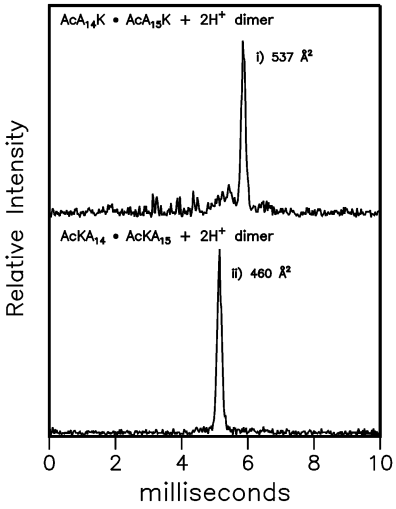

Figure 5. Drift time distributions recorded for the dimer ions obtained from the mixtures of (a) Ac−A_{14}K and Ac−A_{15}K and (b) Ac−KA_{14} and Ac−KA_{15}.

Ac−A_{14}K and Ac−A_{15}K and Ac−KA_{14} and Ac−KA_{15} Mixtures. Figure 4a shows a typical mass spectrum for an Ac−A_{14}K and Ac−A_{15}K mixture recorded using similar conditions to those employed for the measurements shown in Figure 1. There is only a small amount of dimer present. The drift time distribution of the dimer Ac−A_{14}K·Ac−A_{15}K+$2H^+$ in the upper half of Figure 5 is dominated by a single peak. Figure 4b shows a typical mass spectrum for an Ac−KA_{14} and Ac−KA_{15} mixture. The mass spectrum shows a high relative abundance for the Ac−KA_{14}·Ac−KA_{15}+$2H^+$ dimer. Trimers, on the other hand, are absent. We performed some measurements with lower capillary temperatures (28−40 °C), and in some of these studies (two out of six), low intensity peaks were observed in the positions expected for trimers. There is some question as to the assignment of these peaks, and we were not able to find conditions where the trimers could be reproducibly obtained. It is clear that trimers are much less abundant for the polyalanine-based peptides than for the alanine/glycine-based ones. The drift time distribution for the Ac−KA_{14}·Ac−KA_{15}+$2H^+$ dimer in

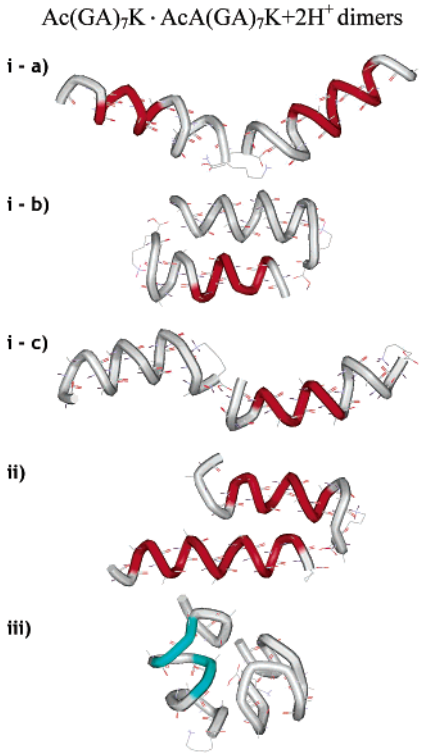

Figure 6. $Ac-(GA)_7K\cdot Ac-A(GA)_7K+2H^+$ dimer conformations obtained from MD simulations. The labels refer to possible assignments to the features in the measured drift time distribution (Figure 2). The images were produced using the WebLab viewer (Molecular Simulations Inc., San Diego, CA). The red regions are α helix, and the blue regions are β sheet.

the lower half of Figure 5 shows a single peak. The results obtained for $Ac-A_{14}K\cdot Ac-A_{15}K+2H^+$ and $Ac-KA_{14}\cdot Ac-KA_{15}+2H^+$ dimers confirm results obtained previously by our group with poorly defined mixtures containing a broad range of $Ac-A_nK$ and $Ac-KA_n$ peptides.[17]

MD for the $Ac-(GA)_7K\cdot Ac-A(GA)_7K+2H^+$ Dimers. Figure 6 shows the low energy conformations found in the MD simulations for the $Ac-(GA)_7K\cdot Ac-A(GA)_7K+2H^+$ dimers. The labels in Figure 6 refer to possible assignments to the features seen in the drift time distribution for the dimer in Figure 2. Table 1 shows a comparison of the cross sections and energies of the various dimer conformations. A V-shaped arrangement of helices with the C termini linked, Figure 6i−a, and a nearly collinear arrangement with N/C termini linked, Figure 6i−c, both have cross sections that are close to that for the dominant feature in the drift time distribution for the $Ac-(GA)_7K\cdot Ac-A(GA)_7K+2H^+$ dimer. The V-shaped arrangement is significantly lower in energy, according to the simulations, and so this is probably the arrangement responsible for the dominant feature in the drift time distribution. Another possible arrangement, with antiparallel helices, Figure 6i−b, has a low energy, but its cross section is a poor match with all of the observed dimer features.

In the V-shaped arrangement, the C termini are linked together with the lysine of one peptide associated with the C terminus of the other, see Figure 6i−a. Unfavorable electrostatic interactions between the helix dipoles are minimized in the V-shaped arrangement. In fact, there is a cooperative electrostatic stabilization of both helices: the helix dipoles of both peptides point toward both charges in this arrangement. This also compensates for the Coulomb repulsion between the two charges which are close together in this arrangement. To dissociate the V-shaped dimer, the protonated lysine side chains must exchange, moving from one peptide to the other to become self-solvated. This probably leads to a significant barrier to dissociation. In fact, the V-shaped dimer survived a 1 ns MD simulations at 600 K, indicating that the exchange process does not occur readily. Although, in the experiments, the dimers can be completely dissociated by raising the capillary temperature to 403 K. The apparent difference between the simulations and experiment may just be a consequence of the different time scales involved. Significant activation barriers are not expected in the dissociation of the other two geometries mentioned above: the antiparallel helices, Figure 6i−b, and the nearly collinear arrangement with N-/C-termini linked, Figure 6i−c. In both these geometries, the lysine side chains are not exchanged (they are self-solvated).

Reorientating the helices in the geometries discussed above leads to higher energy structures. A nearly collinear arrangement of helices such as that shown in Figure 6i−c but with the N termini linked instead of the N/C termini is highly unstable and in most cases dissociates into monomers during the course of the simulations. Although the antiparallel (head-to-toe) arrangement shown in Figure 6i−b has a low energy, the corresponding parallel conformation (head-to-head) does not survive in the simulations. Unfavorable electrostatic interactions between the helix dipoles destabilizes the parallel dimer, and it opens up to a V-shaped arrangement, but without the exchange of the lysine side chains. These nonexchanged species are slightly higher in energy than the exchanged form shown in Figure 6i−a and discussed above.

We now discuss conformations that may be responsible for the two minor features in the dimer drift time distribution. The only conformation found in the MD simulations with an appropriate cross section to account for the second most abundant feature drift time in the drift time distribution is shown in Figure 6ii. This conformation has two helices in a shifted parallel arrangement. Offsetting the helices reduces the unfavorable electrostatic interactions between the helix dipoles. Side chain interactions also help to stabilize this dimer. In the figure, it is evident that the second peptide partially solvates the protonated lysine side chain on the first. The energy of this arrangement is only slightly less favorable that the V-shaped dimer (see Table 1). A globular dimer consisting of two peptides in random-looking arrangements is the only conformation found in the simulations with a cross section that will match that of the least abundant feature in the drift time distribution (which

TABLE 1: Cross Sections and Energies for $Ac-(GA)_7K\cdot Ac-A(GA)_7K+2H^+$ Dimers from MD Simulations and Experiment

$Ac-(GA)_7K\cdot Ac-A(GA)_7K+2H^+$ dimers	cross section, Å^2	energy, kJ mol^{-1}
experiment, dominant feature, Figure 2i	485	
V-shaped, C-termini linked, Figure 6i−a	483	−4493
antiparallel helices, Figure 6i−b	409	−4485
roughly collinear helices, C-/N-termini linked, Figure 6i−c	492	−4448
experiment, secondary feature Figure 2ii	433	
shifted parallel helices, Figure 6ii	437	−4480
experiment, tertiary feature, Figure 2iii	379	
aggregation of two globules, Figure 6iii	380	−4402

TABLE 2: Cross Sections and Energies for Ac−$(GA)_7$K+H^+ and Ac−A$(GA)_7$K+H^+ Trimers from MD Simulations and Experiment

	cross section, Å^2	energy, kJ mol^{-1}
2Ac−$(GA)_7$K·Ac−A$(GA)_7$K+3H^+ trimers		
experiment, dominant feature, Figure 2iv	683	
pinwheel, C-termini together, Figure 7iv	677	−6616
experiment, secondary feature, Figure 2v	624	
V-shaped dimer with antiparallel helix, Figure 7v−a	639	−6615
V-shaped dimer with antiparallel helix, Figure 7v−b	585	−6605
experiment, tertiary feature, Figure 2vi	571	
Ac−$(GA)_7$K·2Ac−A$(GA)_7$K+3H^+ trimers		
experiment, dominant feature, Figure 2vii	696	
pinwheel, C-termini together, Figure 7vii	695	−6742
experiment, secondary feature Figure 2viii	635	
V-shaped dimer with antiparallel helix, Figure 7viii	627	−6753
experiment, tertiary feature, Figure 2ix	571	
three side-by-side helices, Figure 7ix	569	−6703

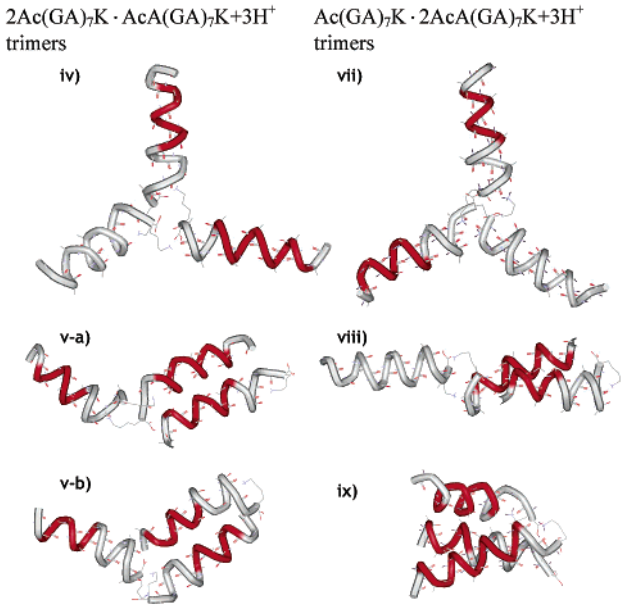

Figure 7. 2Ac−$(GA)_7$K·Ac−A$(GA)_7$K+3H^+ and Ac−$(GA)_7$K·2Ac−A$(GA)_7$K+3H^+ trimer conformations obtained from MD simulations. The labels refer to possible assignments to the features in the measured drift time distributions (Figure 2). The images were produced using the WebLab viewer (Molecular Simulations Inc., San Diego, CA). The red regions are α helix, and the blue regions are β sheet.

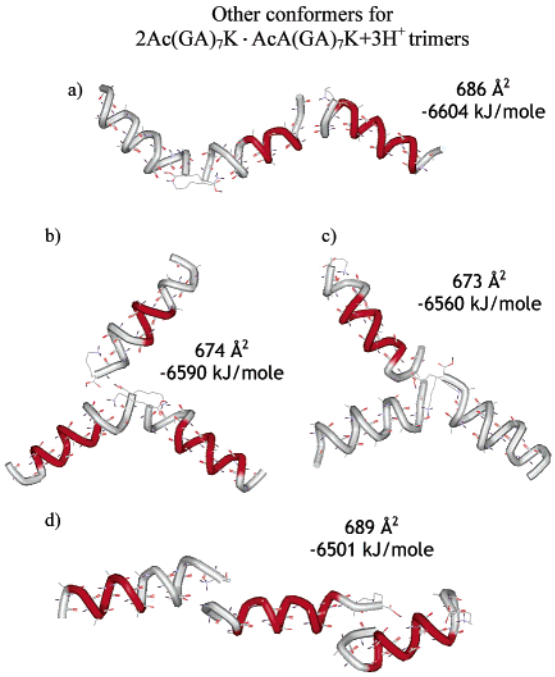

Figure 8. Other conformations which match the cross section for the dominant feature in the drift time distribution of the 2Ac−$(GA)_7$K·Ac−A$(GA)_7$K+3H^+ trimer, Figure 2iv. The images were produced using the WebLab viewer (Molecular Simulations Inc., San Diego, CA). The red regions are α helix, and the blue regions are β sheet.

also has the smallest cross section). It is quite common for one of the peptides to have a short helical section, as in the example shown in Figure 6iii.

MD for the Ac−$(GA)_7$K+H^+ and Ac−A$(GA)_7$K+H^+ Trimers. The number of possible conformations increases dramatically with the addition of a third peptide. However, after examination of the large number of MD simulations performed for the trimers, it became evident that only a few different conformational categories are important. Table 2 contains the cross sections and energies for the most stable conformations that come close to matching the measured cross sections. Figure 7 shows the conformations, labeled to match the cross sections for the features resolved in Figure 2. The conformation that appears to be the best match to the main feature in the drift time distribution has a pinwheel or star-shaped arrangement with the helices radiating out from a central point. Here, all three lysines are exchanged, with each one interacting with a different helix while also contributing to the stabilization of the remaining two helices through cooperative electrostatic interactions (as discussed above for the dimers). The pinwheel arrangement also minimizes the unfavorable electrostatic interactions between the helix dipoles. The pinwheel conformation survived 600 K 960 ps MD simulations without dissociating. Here again, the activation barrier to exchanging the lysines helps to maintain the structure and resist dissociation.

Figure 8 shows some higher energy conformations which come close to matching the cross section for the dominant feature in the drift time distribution for the 2Ac−$(GA)_7$K·Ac−A$(GA)_7$K+3H^+ trimer. Similar results were obtained for the Ac−$(GA)_7$K·2Ac−A$(GA)_7$K+3H^+ trimer. The conformations in Figure 8 all contain a V-shaped dimer with exchanged lysines but differ in the orientation of the third helix which has a self-solvated lysine. Figure 8a shows a roughly collinear configuration which is only slightly higher in energy than the pinwheel configuration. However, like all of the conformations in Figure 8, the roughly collinear configuration dissociates readily in high temperature simulations (losing the helix with the self-solvated lysine). Because of the low barrier to dissociation, these conformations may not be important contributors to the measured drift time distribution. The roughly collinear configuration in Figure 8a lacks the cooperative electrostatic helix-stabilizing interactions present in the pinwheel, but this conformation is stabilized by the helix dipoles in the second and third helices

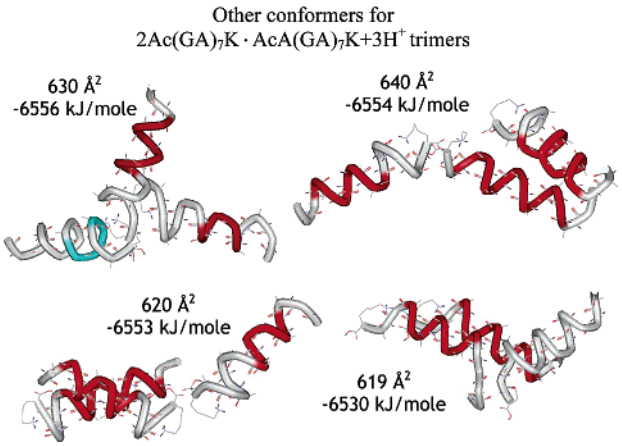

Figure 9. Other conformations which match the cross section for the secondary feature in the drift time distribution of the 2Ac−$(GA)_7$K·Ac−A$(GA)_7$K+$3H^+$ trimer, Figure 2v. The images were produced using the WebLab viewer (Molecular Simulations Inc., San Diego, CA). The red regions are α helix, and the blue regions are β sheet.

pointing in opposite directions. A similar roughly collinear configuration with the second and third helices pointing in the same direction, Figure 8d, is considerably higher in energy. Figure 8 parts b and c are variations on the pinwheel theme. Figure 8b has the C terminus of the third helix pointing toward the center of the pinwheel, whereas Figure 8c has the C terminus pointing away from the center. The former (which has the three charges close to the center of the pinwheel) maximizes the cooperative electrostatic stabilization of the helices, whereas the latter results in more favorable interactions between the helix dipoles. Figure 8b has the lower energy which indicates that the cooperative electrostatic stabilization is the stronger effect. At first glance, this is a little surprising because it is also necessary to overcome the Coulomb repulsion resulting from placing the three charges close together. In the simulations, the third helix in the arrangement shown in Figure 8c often flipped around to give the arrangement in Figure 8b.

Low energy conformations with cross sections close to those of the second most abundant feature in the drift time distributions for the 2Ac−$(GA)_7$K·Ac−A$(GA)_7$K+$3H^+$ and Ac−$(GA)_7$K·2Ac−A$(GA)_7$K+$3H^+$ trimers are shown in Figure 7 parts v−a, v−b, and viii. These conformations are related to the ones discussed above. They have a V-shaped dimer with exchanged lysines and a third helix, which has a self-solvated lysine, oriented in an antiparallel, coiled-coil arrangement with one of the two helices that makeup the vee. These arrangements have energies that are comparable to the pinwheel conformation discussed above (see Table 2). As illustrated by Figure 7 parts v−a and v−b, slightly different arrangements of the V-shaped dimer with antiparallel helix lead to a fairly broad range of cross sections, from slightly larger than the measured value to significantly smaller. Examples of other conformations that come close to matching the cross section for the second feature in the drift time distributions are shown in Figure 9. These are all at least 60 kJ mol^{-1} higher in energy than the V-shaped dimer with antiparallel helix. As can be seen, they are distorted versions of the conformations shown in Figure 7, usually with the lysines of all three monomers self-solvated.

It was difficult to find conformations with cross sections that came close to matching the measured value for the third feature in the drift time distributions of the 2Ac−$(GA)_7$K·Ac−A$(GA)_7$K+$3H^+$ and Ac−$(GA)_7$K·2Ac−A$(GA)_7$K+$3H^+$ trimers. Figure 7ix shows a conformation consisting of three side-by-side helices that matches the measured cross section for the Ac−$(GA)_7$K·2Ac−A$(GA)_7$K+$3H^+$ trimers. Both parallel and antiparallel forms were found and have about the same energy. A similar arrangement did not survive in the MD simulations of the 2Ac−$(GA)_7$K·Ac−A$(GA)_7$K+$3H^+$ trimer. The three side-by-side helices are around 50 kJ mol^{-1} less stable than the pinwheel conformation and the V-shaped dimer with antiparallel helix, and they often converted into these conformations in the simulations.

In view of the large number of conformations that are nearly degenerate in energy, for some of them, we did more simulations at a range of different temperatures in order to gain insight into their stability toward dissociation. As noted above, conformations with all of the lysines exchanged, like the pinwheel conformation in Figure 7 parts iv and vii, survive nanosecond simulations at 600 K. Here we focused on conformations with two helices with exchanged lysines in a V-shape and a third helix with a self-solvated lysine in different orientations. Specifically, we examined a pinwheel conformation, Figure 8b; a V-shaped dimer with antiparallel helix, Figure 7v; and a collinear arrangement, Figure 8a. Two 1 or 2 ns simulations were performed for these starting conformations at 300, 320, 340, 360, 380, 400, 500, and 600 K. The collinear form dissociated at 340 K, and the pinwheel dissociated at 380 K. The V-shaped dimer with antiparallel helix was the most stable, it did not dissociate until the temperature was raised to above 400 K.

MD for the Ac−K$(GA)_7$+H^+ and Ac−KA$(GA)_7$+H^+ Multimers. Table 3 contains the cross sections and energies for the most stable conformations that come close to matching the measured cross sections. Figure 10 shows the conformations, labeled to match the cross sections for the features resolved in Figure 3. The only conformations found in the simulations that were compact enough to match the measured cross sections for the dominant features in the drift time distributions of the Ac−K$(GA)_7$+H^+ and Ac−KA$(GA)_7$+H^+ dimers and trimers were globules. For the Ac−K$(GA)_7$·Ac−KA$(GA)_7$+$2H^+$ dimer, the second most abundant feature in the drift time distribution can be accounted for by a conformation with antiparallel helices with exchanged lysines, Figure 10ii. According to the simulations, this conformation is around 100 kJ mol^{-1} more stable than the dimer globule, Figure 10i, even though it is the less abundant feature in the drift time distribution. The dimer globule in Figure 10i is actually around 84 kJ mol^{-1} higher than the sum of the energies of the lowest energy monomer conformations (which are also globules). It is difficult to find the lowest energy conformation for a globule because so many different conformations are possible. The difficulty increases rapidly with size, and so it is much more difficult to locate the lowest energy structure for the dimer globule than it is for the monomer globules. Low energy dimer globules can be constructed by gently pushing together the lowest energy monomer globules. The resulting conformations, however, are elongated and do not match the measured cross section for the dominant feature in the drift time distribution. We anticipate that there are compact conformations for the dimer globules that are marginally more stable than the isolated dimers, but they have just not been found.

For the 2Ac−K$(GA)_7$·Ac−KA$(GA)_7$+$3H^+$ and Ac−K$(GA)_7$·2Ac−KA$(GA)_7$+$3H^+$ trimers, the second most abundant feature in the drift time distributions can be accounted for by aggregates of helices and globules: two helices and a globule or a helix and two globules, see Figure 10 parts iv and vi. The term globule is used rather loosely here because the unfolded peptide is often partly draped around the remaining helices. The energies of the aggregates are about 100 kJ mol^{-1} higher than the sum of the

TABLE 3: Cross Sections and Energies for Ac−K(GA)$_7$+H$^+$ and Ac−KA(GA)$_7$+H$^+$ Multimers from MD Simulations and Experimnt

	cross section, A^2	energy, kJ mol^{-1}
Ac−K(GA)$_7$·A−KA(GA)$_7$+2H$^+$ dimers		
experiment, dominant feature, Figure 3i	380	
globular, from parallel extended linear chains, Figure 10i	376	−4335
experiment, secondary feature, Figure 3ii	410	
antiparallel helices with exchanged lysines, Figure 10ii	420	−4436
2Ac−K(GA)$_7$·Ac−KA(GA)$_7$K+3H$^+$ trimers		
experiment, dominant feature, Figure 3iii	503	
globular, from three globules, Figure 10iii	519	−6461
experiment, secondary feature, Figure 3iv	564	
aggregate of two helices and a globule, Figure 10iv	570	−6493
Ac−K(GA)$_7$·2Ac−KA(GA)$_7$K+3H$^+$ trimers		
experiment, dominant feature, Figure 3v	520	
globular, from three globules, Figure 10v	528	−6572
experiment, secondary feature, Figure 3vi	575	
aggregate of a helix and two globules, Figure 10vi	569	−6568

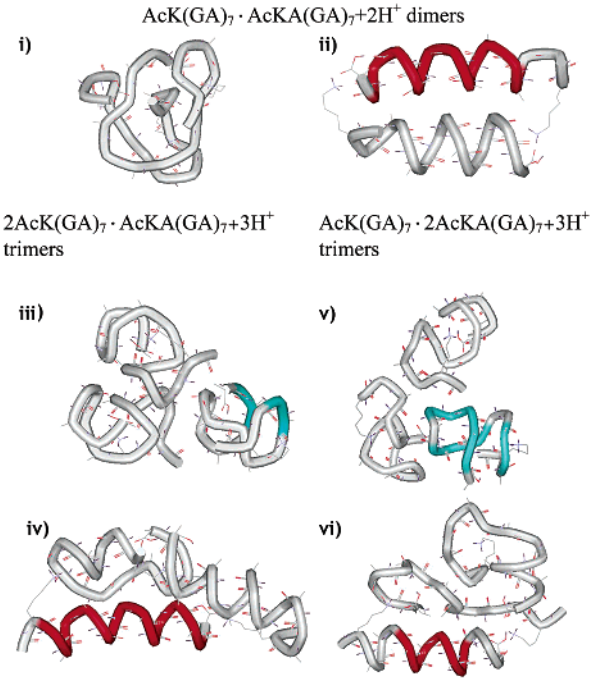

Figure 10. Ac−K(GA)$_7$K+H$^+$ and Ac−KA(GA)$_7$K+H$^+$ dimer and trimer conformations obtained from MD simulations. The labels refer to possible assignments to the features in the measured drift time distributions (Figure 3). The images were produced using the WebLab viewer (Molecular Simulations Inc., San Diego, CA). The red regions are α helix, and the blue regions are β sheet.

energies of the monomeric globules. Not surprisingly, the same difficulties described above in finding low energy dimeric aggregations of globules are also present when investigating the trimers. The aggregates formed in simulations started from three helices, one or two of the helices unfolded during the course of the simulation. For isolated Ac−K(GA)$_7$+H$^+$ and Ac−KA(GA)$_7$+H$^+$, simulations started from an ideal α helix always unfolded to globules. The aggregates have cross sections that are close to those for the third and least abundant feature in the drift time distributions of the 2Ac−(GA)$_7$K·Ac−A(GA)$_7$K+3H$^+$ and Ac−(GA)$_7$K·2Ac−A(GA)$_7$K+3H$^+$ trimers. As described above, a conformation consisting of three side by side helices, Figure 7ix, comes close to matching the measured cross sections, but it readily converts into other conformations. Conformations such as the aggregates discussed here provide another possible explanation for the small feature in the drift time distributions of the 2Ac−(GA)$_7$K·Ac−A(GA)$_7$K+3H$^+$ and Ac−(GA)$_7$K·2Ac−A(GA)$_7$K+3H$^+$ trimers. Comparison of the energies in Tables 2 and 3, however, suggests that this aggregate will be a relatively high energy conformation for the 2Ac−(GA)$_7$K·Ac−A(GA)$_7$K+3H$^+$ and Ac−(GA)$_7$K·2Ac−A(GA)$_7$K+3H$^+$ trimers.

MD for the Ac−A$_{14}$K·Ac−A$_{15}$K+2H$^+$ and Ac−KA$_{14}$·Ac−KA$_{15}$+2H$^+$ Dimers. Table 4 lists values for cross sections and energies for conformations that come close to matching the measured cross sections shown in Figure 5. The conformations are shown in Figure 11. For the Ac−A$_{14}$K·Ac−A$_{15}$K+2H$^+$ dimer, a V-shaped dimer with exchanged lysines, Figure 11i, is a good match with the measured cross section. Another V-shaped arrangement with one of the helices flipped around so that the helix dipoles are aligned (see Table 4) also matches the measured cross sections, but it is considerably higher in energy in the simulations because this conformation has lost the cooperative electrostatic stabilization of the helices. A conformation with antiparallel helices is close in energy to the V-shaped dimer with exchanged lysines, but its cross section is not a good match with the measured value. On the other hand, a conformation with antiparallel helices, Figure 11ii, is a good match to the measured cross section for the Ac−KA$_{14}$·Ac−KA$_{15}$+2H$^+$ dimer. A globular dimer is both higher in energy than the conformation with two antiparallel helices and has a cross section that does not match the measured value.

Helix Packing. The antiparallel dimers in Figures 6i−b, 10ii, and 11ii, the trimers in Figure 7 parts v, viii, and ix, and three of the trimers in Figure 9 contain coiled-coil type arrangements. The angles between the helix axes are typically ∼20°. Figure 11ii shows two views of the Ac−KA$_{14}$·Ac−KA$_{15}$+2H$^+$ dimer illustrating the typical relative orientation of the helices. The packing of helices is usually described by either the "knobs in holes"[32] model or the "ridges into grooves"[33] model. These models differ in their residue−residue interactions and the interhelix angles (18° for the "knobs in holes" model and ∼20°, ∼50°, or ∼80° for the "ridges into grooves"). Although there is considerable variability in the observed aggregates, the "ridges in grooves" model is more appropriate for the majority of structures. In some cases, helix−helix angles of 40−50° were found, which is consistent with the second class within the "ridges into grooves" model. Compared to the peptides with no glycines, incorporation of the glycines was found to consistently reduce the distance between the axes of the helices in the coiled-coil configuration. The average distance between axes of peptides with no glycines was 8.5 Å compared to 7.5 Å for the peptides with glycines. This is in the range of interhelical distances found in natural coiled-coil proteins.[34]

Relative Energies of Multimers versus Monomers. The lowest energy Ac−(GA)$_7$K·Ac−A(GA)$_7$K+2H$^+$ dimer conformation found in the simulations, Figure 6i−a, is around 34 kJ

TABLE 4: Cross Sections and Energies for $Ac-A_{14}K\cdot Ac-A_{15}K+2H^+$ and $Ac-KA_{14}\cdot Ac-KA_{15}+2H^+$ Dimers from MD Simulations and Experiment

	cross section, A^2	energy, kJ mol^{-1}
$Ac-A_{14}K\cdot Ac-A_{15}K+2H^+$ dimers		
experiment, dominant feature, Figure 5i	537	
V-shaped, C-termini together, exchanged lysines, Figure 11i	530	−4507
V-shaped, C-/N-termini together, self-solvated lysines	539	−4363
antiparallel helices, self-solvated lysines	457	−4433
$Ac-A_{14}K\cdot Ac-KA_{15}+2H^+$ dimers		
experiment, dominant feature, Figure 5ii	460	
antiparallel helices, exchanged lysines, Figure 11ii	467	−4460
globular, from parallel extended linear chains	429	−4402

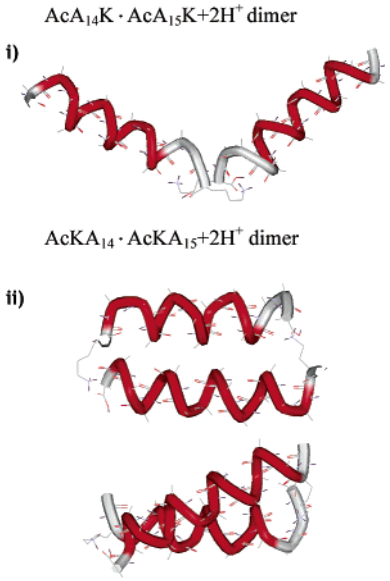

Figure 11. $Ac-A_{14}K\cdot Ac-A_{15}K+2H^+$ and $Ac-KA_{14}\cdot Ac-KA_{15}+2H^+$ dimer conformations obtained from MD simulations. The labels refer to possible assignments to the features in the measured drift time distributions (Figure 5). The images were produced using the WebLab viewer (Molecular Simulations Inc., San Diego, CA). The red regions are α helix, and the blue regions are *β* sheet. Two views of the structure in (ii) are shown to illustrate the coiled-coil geometry.

mol^{-1} lower than the sum of the energies of the lowest energy isolated monomers. For the $Ac-A_{14}K\cdot Ac-A_{15}K+2H^+$ dimer, the energy of the lowest energy conformation, Figure 11i, is 24 kJ mol^{-1} lower than the sum of the monomers These values are not free energies, however. When two monomers form a dimer, there is invariably an entropic penalty that results primarily from the substantial loss of translational entropy. The lost translational entropy can be estimated from statistical mechanics to be ∼200 J K^{-1} mol^{-1}, which leads to a $T\Delta S$ term term of ∼60 kJ mol^{-1} at room temperature. Thus, it appears that the isolated monomers should be ∼30 kJ mol^{-1} more stable than the dimer. Although the preceding is only a rough estimate, it is evident that the contribution of the entropy will significantly reduce, or even reverse, the relative stability of the dimer compared to the monomer. The energies of the $2Ac-(GA)_7K\cdot Ac-A(GA)_7K+3H^+$ and $Ac-(GA)_7K\cdot 2Ac-A(GA)_7K+3H^+$ trimers are slightly (<10 kJ mol^{-1}) higher in energy than the isolated monomers. However, the substantial entropic penalty for trimer formation will lead to a large positive free energy change for assembling the trimers.

The multimers observed in the experiments are not formed in the gas phase, and they are probably present in solution and transferred into the gas phase (though the possibility of them forming during the electrospray process cannot be completely ruled out). Thus, the kinetic stability of the multimers rather than their thermodynamic stability determines whether they are observed. As we have already discussed, conformations with exchanged lysines (like the lowest energy $Ac-(GA)_7K\cdot Ac-A(GA)_7K+2H^+$ and $Ac-A_{14}K\cdot Ac-A_{15}K+2H^+$ dimers discussed above) are expected to have significant activation barriers associated with their dissociation.

For dimers of peptides with the lysine at the N terminus the situation is quite different. For the $Ac-KA_{14}\cdot Ac-KA_{15}+2H^+$ dimer, the energy of the lowest energy conformation is 153 kJ mol^{-1} lower than the isolated monomers. In this case, the dimer conformation has antiparallel helices with exchanged lysines, whereas the monomers are globules. In the monomer, the helix is destabilized by the N-terminus lysine, but in the dimer, helix formation is promoted because with an antiparallel arrangement of helices the N-terminus lysine of one peptide is able to interact with the C-terminus of the other. The dimer is stabilized by the formation of the helices. For the $Ac-K(GA)_7\cdot Ac-KA(GA)_7+2H^+$ dimer, the analogous conformation is only around 17 kJ mol^{-1} more stable than the isolated monomers (which are also globules) because the glycines destabilize the helical state. For this reason, the antiparallel helix is not the dominant feature in the drift time distribution for the $Ac-K(GA)_7\cdot Ac-KA(GA)_7+2H^+$ dimer. The dominant feature is a globular dimer.

In the experiments, the relative abundance of the $Ac-KA_{14}\cdot Ac-KA_{15}+2H^+$ dimer is substantially greater than for the $Ac-K(GA)_7\cdot Ac-KA(GA)_7+2H^+$ dimer. The high relative abundance of the $Ac-KA_{14}\cdot Ac-KA_{15}+2H^+$ dimer can be explained by its high stability, which was discussed above. There is not an obvious explanation for the virtual absence of trimers from the $Ac-KA_{14}$ and $Ac-KA_{15}$ mixture. For peptides with the lysine at the C terminus, the $Ac-(GA)_7K\cdot Ac-A(GA)_7K+2H^+$ dimer is more abundant than the $Ac-A_{14}K\cdot Ac-A_{15}K+2H^+$ dimer. This is the a reverse of the trend observed for the peptides with the N-terminus lysine. Again, trimers are only observed for the peptides that contain glycine. Explanations for these observations are not evident from the simulations.

Conclusions

The helix-forming monomers, $Ac-A_{14}K$ and $Ac-A_{15}K$ and $Ac-(GA)_7K$ and $Ac-A(GA)_7K$, primarily form V-shaped dimers. Other conformations (shifted parallel helices and dimer globule) are present for the $Ac-(GA)_7K\cdot Ac-A(GA)_7K+2H^+$ dimer but not for $Ac-A_{14}K\cdot Ac-A_{15}K+2H^+$. The dominant conformation present for the trimers of the peptides with glycine are pinwheels. A conformation consisting of a V-shaped dimer with a third helix orientated antiparallel occurs with lower abundance. The V-shaped dimer and pinwheel trimer have their charged groups localized together (an arrangement which at first glance seems unfavorable). However, this leads to a cooperative electrostatic stabilization of the helices through the interaction of the combined charge with the helix dipoles. According to the simulations, the charge localization and cooperative stabilization are more important than having the most favorable

alignment of the helix dipoles. Using relative energies from the simulations, the free energy changes for multimer formation are expected to be positive (due at least partly to a significant entropic penalty for multimer formation). However, there are expected to be significant activation barriers associated with dissociating the V-shaped dimer and pinwheel trimer because the lysines are exchanged (the protonated lysine from one peptide interacts with the C terminus of another) and must be rearranged before dissociation can occur.

The peptides with the lysine at the N terminus form globules in the monomeric state because the helix is destabilized by unfavorable interactions between the charge and the helix dipole. The abundant $Ac-KA_{14}\cdot Ac-KA_{15}+2H^+$ has a conformation with antiparallel helices where the N-terminus lysine on one peptide interacts with the C terminus of the other. This conformation is also observed for the $Ac-K(GA)_7\cdot Ac-KA(GA)_7+2H^+$ dimer, but it is not the main feature in the drift time distribution. The most abundant conformation is a dimer globule because the glycines destabilize the helical state in the $Ac-K(GA)_7\cdot Ac-KA(GA)_7+2H^+$ dimer. The globule is also the most abundant conformation for the trimers from the $Ac-K(GA)_7$ and $Ac-KA(GA)_7$ mixture. Conformations with one or more helices were present as well. Here the helices are stabilized by interactions with their local environment.

Acknowledgment. We thank Jiri Kolafa for the use of his MACSIMUS molecular modeling programs. We gratefully acknowledge the support of the National Institutes of Health.

References and Notes

(1) Dill, K. A. *Biochemistry* **1990**, *29*, 7133−7155.
(2) Wallin, E.; von Heijne, G *Protein Sci.* **1998**, *7*, 1029−1038.
(3) For some examples of studies of unsolvated peptides and proteins, see: Suckau, D.; Shi, Y.; Beu, S. C.; Senko, M. W.; Quinn, J. P.; Wampler, F. M.; McLafferty, F. W. *Proc. Natl. Acad. Sci.* **1993**, *90*, 790−793. Campbell, S.; Rodgers, M. T.; Marzluff, E. M.; Beauchamp, J. L. *J. Am. Chem. Soc.* **1995**, *117*, 12840−12854. Schnier, P. D.; Price, W. D.; Jockusch, R. A.; Williams, E. R. *J. Am. Chem. Soc.* **1996**, *118*, 7178−7189. Kaltashov, I. A.; Fenselau, C. *Proteins: Struct. Func. Genet.* **1997**, *27*, 165−170. Valentine, S. J.; Clemmer, D. E. *J. Am. Chem. Soc.* **1997**, *119*, 3558−3566. Wyttenbach, T., Bushnell, J. E.; Bowers, M. T. *J. Am. Chem. Soc.* **1998**, *120*, 5098−5103. Arteca, G. A.; Velázquez, I.; Reimann, C. T.; Tapia, O. *Phys. Rev. E* **1999**, *59*, 5981−5986. Schaaff, T. G.; Stephenson, J. L.; McLuckey, S. L. *J. Am. Chem. Soc.* **1999**, *121*, 8907−8919.
(4) Hudgins, R. R.; Mao, Y.; Ratner, M. A.; Jarrold, M. F. *Biophys. J.* **1999**, *76*, 1591−1597.
(5) Kinnear, B. S.; Jarrold, M. F. *J. Am. Chem. Soc.* **2001**, *123*, 7907−7908.
(6) Branden, C., Tooze, J. *Introduction to Protein Structure*, 2nd ed.; Garland: New York, 1999.
(7) Sansom, M. S. P. *Prog. Biophys. Mol. Biol.* **1991**, *55*, 139−236.
(8) Kerr, I. D.; Sankararamakrishnan, R.; Smart, O. S.; Sansom, M. S P *Biophys. J.* **1994**, *67*, 1501−1535.
(9) Randa, H. S.; Forrest, L. R.; Voth, G. A.; Sansom, M. S. P *Biophys. J.* **1999**, *77*, 2400−2410.
(10) Pandey, R. C.; Meng, H.; Cook, J. C., Jr.; Rinehart, K. L., Jr. *J. Am. Chem. Soc.* **1977**, *99*, 5203−5205.
(11) Fenn, J. B.; Mann, M.; Meng, C. K.; Wong, S. F.; Whitehouse, C. M. *Science* **1989**, *246*, 64−71.
(12) Light-Wahl, K. J.; Schwartz, B. L.; Smith, R. D. *J. Am. Chem. Soc.* **1994**, *116*, 5271−5278.
(13) Loo, J. *Int. J. Mass Spectrom.* **2000**, *200*, 175−186.
(14) Smith, R. D. *Int. J. Mass Spectrom.* **2000**, *200*, 509−544.
(15) Counterman, A. E.; Valentine, S. J.; Srebalus, C. A.; Henderson, S. C.; Hoagland, C. S.; Clemmer, D. E. *J. Am. Soc. Mass Spectrom.* **1998**, *9*, 746−759.
(16) Lee, S.-W.; Beauchamp, J. L. *J. Am. Soc. Mass Spectrom.* **1999**, *10*, 347−351.
(17) Hudgins, R. R.; Jarrold, M. F. *J. Am. Chem. Soc.* **1999**, *121*, 3494−3501.
(18) Hudgins, R. R.; Ratner, M. A.; Jarrold, M. F. *J. Am Chem. Soc.* **1998**, *120*, 12974−12975.
(19) Kaleta, D. T.; Jarrold, M. F. *J. Phys. Chem. B* **2001**, *105*, 4436−4440.
(20) Kaleta, D. T.; Jarrold, M. F. *J. Am. Chem. Soc.* **2002**, *124*, 1154−1155.
(21) Kinnear, B. S.; Hartings, M. R.; Jarrold, M. F. *J. Am. Chem. Soc.* **2001**, *123*, 5660−5667.
(22) Mason, E. A.; McDaniel, E. W. *Transport Properties of Ions in Gases*; Wiley: New York, 1988.
(23) http://www.icpf.cas.cz/jiri/macsimus/default.htm.
(24) Brooks, B. R.; Bruccoleri, R. E.; Olafson, B. D.; States, D. J.; Swaminathan, S.; Karplus, M. *J. Comput. Chem.* **1983**, *4*, 187−217.
(25) Van Gunsteren, W. F.; Berendsen, H. *J. Mol. Phys.* **1977**, *34*, 1311−1327.
(26) Weiner, S. J.; Kollman, P. A.; Case, D. A.; Singh, U. C.; Ghio, C.; Alagona, G.; Profeta, S.; Weiner, P. *J. Am. Chem. Soc.* **1984**, *106*, 765−784.
(27) Kirkpatrick, S.; Gelatt, C. D., Jr.; Vecchi, M. P. *Science* **1983**, *220*, 671−680.
(28) Kinnear, B. S.; Kaleta, D. T.; Kohtani, M.; Hudgins, R. R.; Jarrold, M. F. *J. Am. Chem. Soc.* **2000**, *122*, 9243−9256.
(29) Presa, L. G.; Rose, G. D. *Science* **1988**, *240*, 1632−1641.
(30) Seale, J. W.; Srinivasan, R.; Rose, G. D. *Protein Sci.* **1994**, *3*, 1741−1745.
(31) Lee, S.-W.; Beauchamp, J. L. *J. Am. Soc. Mass Spectrom.* **1999**, *10*, 347−351.
(32) Crick, F. H. C. *Acta Crystallogr.* **1953**, *6*, 689−697.
(33) Chothia, C.; Levitt, M.; Richardson, D. *Proc. Natl. Acad. Sci U.S.A.* **1977**, *74*, 4130−4134.
(34) Gernert, K. M.; Surles, M. C.; Labean, T. H.; Richardson, J. S.; Richardson, D. C. *Prot. Sci.* **1995**, *4*, 2252−2260.